Multi-way modelling of oral microbial dynamics and host-microbiome interactions during induced gingivitis

G.R. van der Ploeg[1], B.W. Brandt[2], B.J.F. Keijser[3], M.H. van der Veen[2,4], C.M.C. Volgenant[2,5], E. Zaura[2], A.K. Smilde[1], J.A. Westerhuis[1], A. Heintz-Buschart[1*]

[1] *Biosystems Data Analysis, Swammerdam Institute for Life Sciences, University of Amsterdam, Amsterdam, The Netherlands*

[2] *Preventive Dentistry, Academic Centre for Dentistry, Vrije Universiteit Amsterdam and University of Amsterdam, Amsterdam, The Netherlands*

[3] *Microbiology and Systems Biology, TNO Healthy Living and Work, Leiden, The Netherlands*

[4] *Paediatric Dentistry, Academic Centre for Dentistry, Vrije Universiteit Amsterdam and University of Amsterdam, Amsterdam, The Netherlands*

[5] *Cariology, Academic Centre for Dentistry, Vrije Universiteit Amsterdam and University of Amsterdam, Amsterdam, The Netherlands*

*Author for correspondence: Anna Heintz-Buschart a.u.s.heintzbuschart@uva.nl

Geert Roelof van der Ploeg:	https://orcid.org/0009-0007-5204-3386
Monique van der Veen:	https://orcid.org/0000-0002-6844-4682
Bart Keijser:	https://orcid.org/0000-0003-1597-2948
Catherine Volgenant:	https://orcid.org/0000-0002-4049-2914
Bernd Brandt:	https://orcid.org/0000-0002-1155-1989
Egija Zaura:	https://orcid.org/0000-0003-1432-6194
Age Smilde:	https://orcid.org/0000-0002-3052-4644
Johan Westerhuis:	https://orcid.org/0000-0002-6747-9779
Anna Heintz-Buschart:	https://orcid.org/0000-0002-9780-1933

Abstract

Gingivitis - the inflammation of the gums - is a reversible stage of oral disease progression. It is caused by dental plaque formation due to poor oral hygiene. However, gingivitis susceptibility involves a complex set of interactions between the oral microbiome, oral metabolome and the host.

In this study, we investigated the dynamics of the oral microbiome and its interactions with the salivary metabolome during experimental gingivitis in a cohort of 41 systemically healthy participants. We use Parallel Factor Analysis (PARAFAC), which is a multi-way generalization of Principal Component Analysis (PCA) that can model the variability in the response due to subjects, variables and time. Using the modelled responses, we identified microbial subcommunities with similar dynamics that connect to the magnitude of the gingivitis response. By performing high level integration of the predicted metabolic functions of the microbiome and salivary metabolome, we identified pathways of interest that describe the changing proportions of Gram-positive and Gram-negative microbiota, variation in anaerobic bacteria, biofilm formation and virulence.

Key Words

Longitudinal data, Salivary metabolomics, Parallel Factor Analysis, Data integration, Pathway enrichment analysis

Introduction

Microbial oral diseases such as dental caries and gum inflammation are a global public health burden[1–3]. Together, they are the most prevalent health condition world-wide, impacting quality of life and imposing a significant economic burden with 5-10% of public health expenditure in most industrialized countries[3,4]. Prevention of oral diseases is therefore of critical importance.

Gingivitis is a reversible stage of oral disease progression marked by inflamed, bleeding gums[5–7]. It is caused by dental plaque accumulation due to poor oral hygiene[8,9] and is present in a substantial part of the global population[3,10]. The pathogenesis of gingivitis involves a complex set of interactions between the oral microbiome, the oral metabolome and the host[5,11]. These are in turn dependent on many factors[11,12], including host diet[13], life-style[14], and genetics[15]. Failing toothbrushing, which removes plaque and prevents inflammation, results in a high degree of individual variation in gingivitis susceptibility[5,6,11,16–18]

While there is no monocausal microbial agent in gingivitis, the sub-gingival microbiota - underneath the gums - shifts to a dysbiotic state[7]. For example, the depletion of Gram-positive bacteria such as *Rothia dentocariosa* and enrichment in Gram-negative bacteria such as *Porphyromonas gingivalis*, *Prevotella* spp. and *Selenomonas* spp. is frequently observed in case-control comparisons[5,7,19,20]. Additionally, increasing subgingival anaerobiosis during gingivitis progression promotes the growth of pathogens[7,21,22].

Being the medium through which the host and the microbiome interact, the salivary metabolome is often studied as a non-invasive diagnostic of oral disease[23,24]. A well-known host-microbiome interaction is the relation between host sugar consumption and the production of acids by the dental plaque microbiota. This lowers the local pH and shifts the microbiota further towards dysbiosis[25,26]. However, many other dynamic microbe-microbe and host-microbiome interactions that occur throughout gingivitis onset and progression are not well understood.

Here we investigate the spatially resolved oral microbiome and its interactions with the salivary metabolome during experimental gingivitis to (1) identify microbial subcommunities with common dynamics and (2) pinpoint potential impacts on biochemical pathways. Reversible gingivitis was induced in a cohort of 41 systemically healthy participants by omission of oral hygiene during a two-week gingivitis challenge[18,27] (**Figure 1A**). Previously reported plaque levels, gingival bleeding upon probing, and red fluorescent plaque quantification allowed grouping of the participants into identified low, mid and high responders based on the last day of the intervention[18] (**Figure 1B**). During a two-week baseline period at two time points (day -14 and day 0), a challenge period at four time points (day 2 to day 14), and one week resolution period at one time point (day 21), the oral microbiome was determined at six sites: tongue, saliva, supragingival plaque at the lower and upper lingual surfaces and supragingival plaque at the lower and upper interproximal surfaces (**Figure 1C**). To identify the individual variation in the time-resolved response of the oral microbiome to the challenge and describe commonly responding (groups of) microbiota, we employ Parallel Factor Analysis[28,29] (PARAFAC), for modelling the subjects, time, and microbial abundances at each site (**Figure 1D**). The salivary metabolome dynamics, assessed in unstimulated saliva during the challenge, is likewise modelled and integrated with microbiome models at the biochemical pathway level. These analyses should yield insights into microbial processes that underlie individual gingivitis responses.

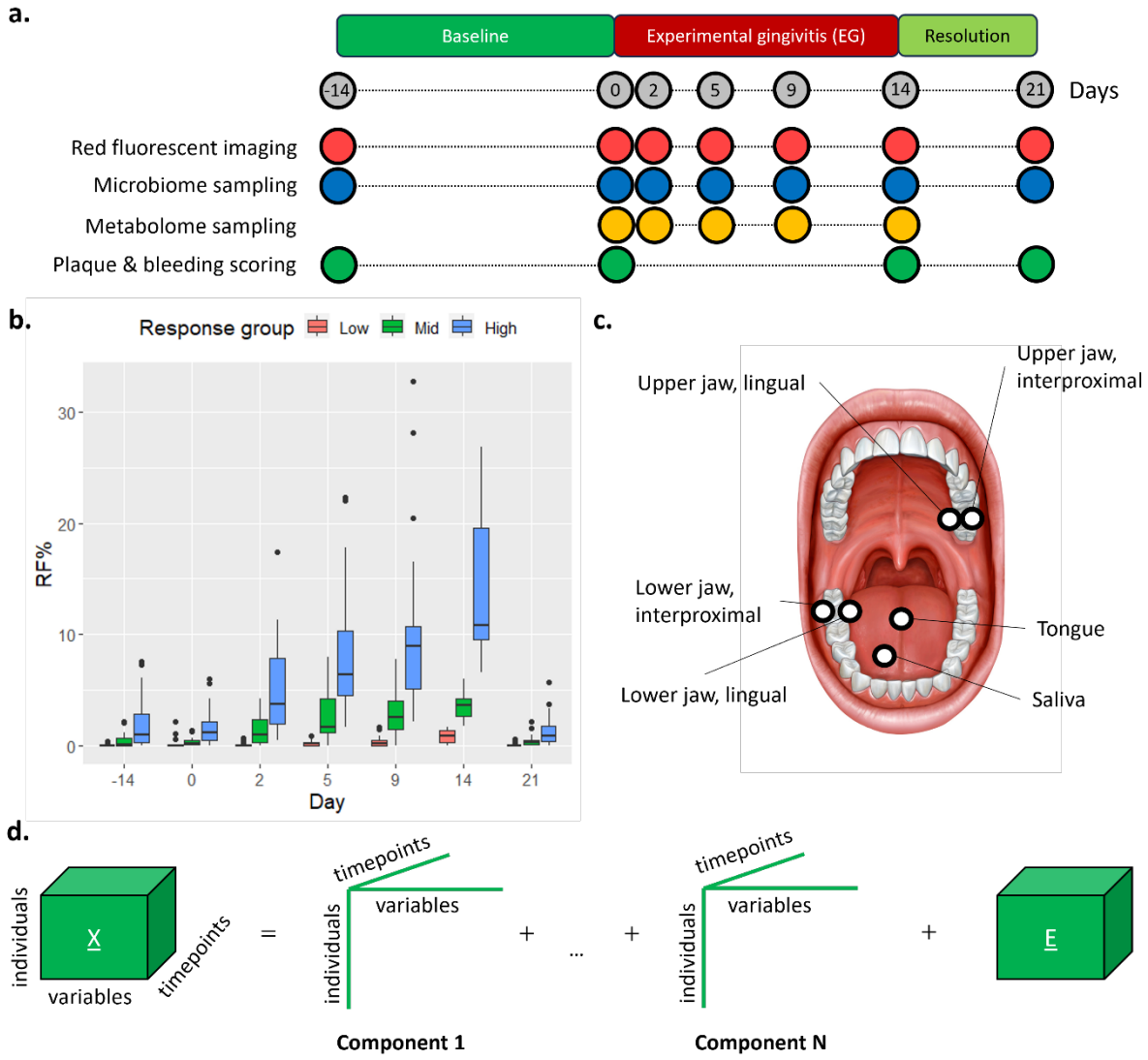

Figure 1: Overview of the study design and analysis. (a) Timeline of experimental gingivitis challenge with analyses; (b) gingivitis responses: Three groups of responders were identified based on red fluorescent dental plaque (RF%) at day 14: low (0-1.7%), mid (1.8-6.0%) and high (6.0%+); (c) oral sampling sites; (d) data analysis approach: Parallel factor analysis (PARAFAC), a multi-way generalization of Principal Component analysis, decomposes a multi-way data cube into components with three loading vectors each: one for the subjects, one for the variables (here: microbial relative abundances) and one for time. This approach allows us to identify the individual variation in the time-resolved response to the challenge and to describe commonly responding groups of microbiota.

Results

PARAFAC describes clinically relevant variation in oral microbiomes between subjects

To describe the microbial dynamics of each oral site for all subjects across time, we analysed 16S rRNA gene amplicon sequencing data for a total of 14,014 amplicon sequence variants (ASVs). After removal of sparse ASVs, we created separate PARAFAC models for each oral site, choosing the most appropriate number of PARAFAC components by inspecting the number of iterations needed to converge[30], the core consistency diagnostic[31], the variation explained[30], and the tucker congruence coefficient per mode[32,33] (**Supplementary Data**). This yielded two-component models for the upper jaw lingual plaque (19.7% explained variation) and upper jaw interproximal plaque (16.5%), tongue (31.5%) and saliva (17.5%) microbiomes (**Figure 2**). Lower jaw lingual and interproximal plaque microbiomes were best represented by one-component models (explaining 11.4% and 7.2% of the variation, respectively). The latter model was not investigated further due to the limited amount of explained variation.

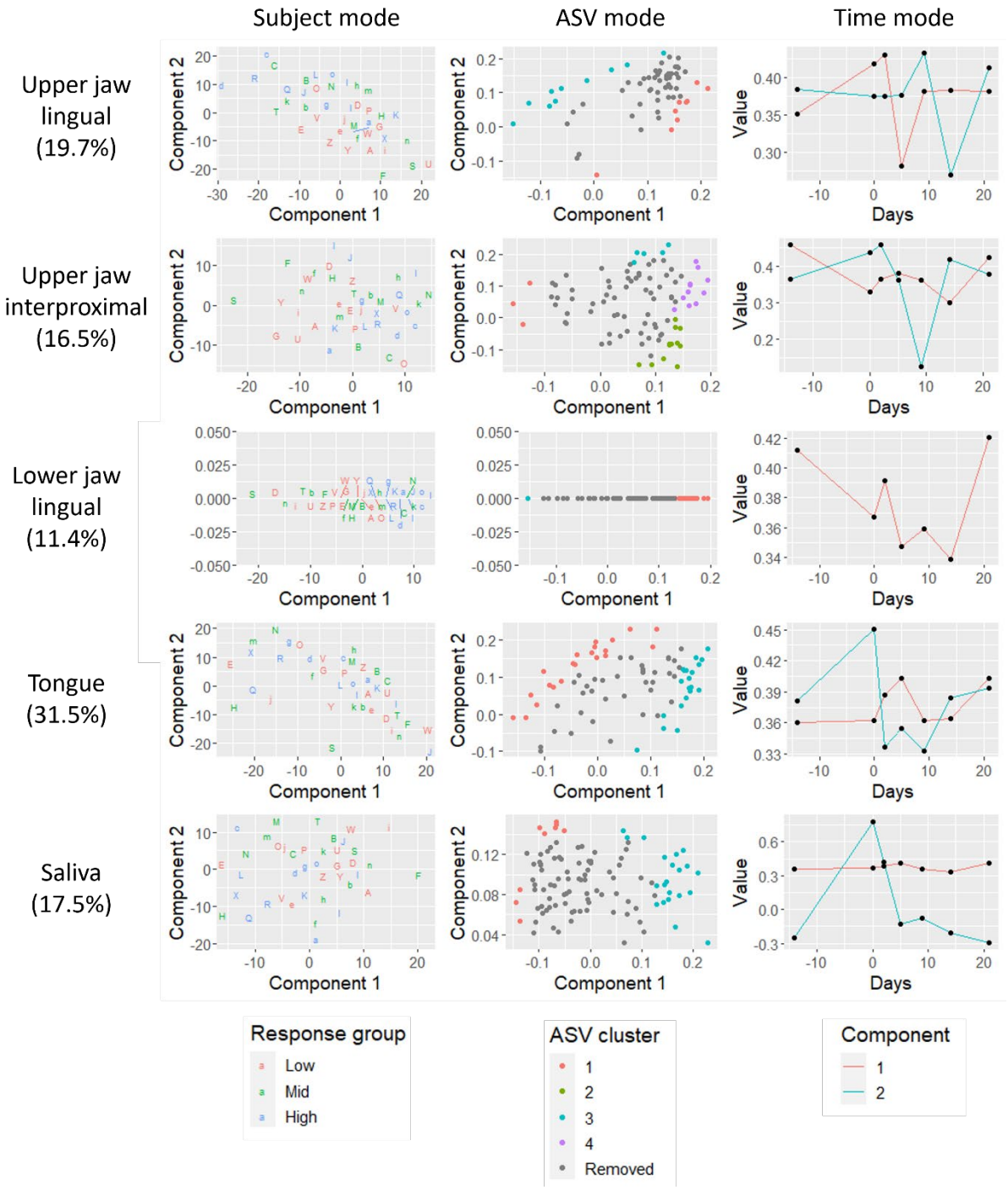

*Figure 2: Overview of the PARAFAC models per sample type. In the left column the loadings of the first and second component in the subject mode are shown, with every subject having a unique character to identify them across the sample types. In the middle column the loadings of the first and second component in the ASV mode are shown. Here ASVs are coloured by their similarly responding cluster after filtering (**Table 2**). In the right column, the loadings per time point are shown. In the rows, the PARAFAC models per sample type are described: upper jaw lingual plaque, upper jaw interproximal plaque, lower jaw lingual plaque, tongue and saliva. Variance explained per model are shown in the sample type labels. The model corresponding to the lower jaw interproximal plaque is not shown due to having limited explained variation. The model corresponding to the lower jaw lingual plaque only has one component.*

To interpret the models, we tested the correlation between the time-resolved subject loadings of each component with the measured parameters of gingivitis. This approach revealed correlation of components with one or more clinical parameter for the three plaque microbiomes (**Table 1**). Overall, the PARAFAC models describe the variation that exists between subjects, rather than the variation within a subject (One-sided Wilcoxon rank-sum test: p=0.020, **Supplementary Figures A1 and A2**). Furthermore, subject age was found to be significantly described by the first component of the model corresponding to the tongue microbiome samples (p=0.035) and the second component of the model corresponding to the saliva microbiome samples (p=0.038) (**Supplementary Table B1**). Gender was not significantly described by any model (**Supplementary Table B1**). We also performed Pearson correlation tests of the time-resolved subject loadings per component with richness and evenness. All microbiome models were found to contain at least one component that significantly described richness or evenness ($p \leq 0.05$; **Table 1**). In conclusion, the PARAFAC models represented clinically and ecologically relevant parameters.

PARAFAC describes microbial subcommunities with common gingivitis responses

Building on the interpretability of the subject modes (**Table 1**), we identified microbial subcommunities with common responses per sampling site by selecting and then clustering well-modelled ASVs based on their fitted response (**Figure 2**, for cluster membership see **Table 2**). The sum of the relative abundances of the ASVs in each cluster was then determined to test the difference between the microbiomes of individuals in the low and high response groups at every time point per oral site (Benjamini-Hochberg corrected permutation test of mean difference: $p \leq 0.05$; **Supplementary Table B2)**. This approach revealed significant differences in the relative abundance of most plaque-associated ASV clusters in high responders compared to the low responders at baseline (day -14; **Figure 3**, **Supplementary Figure A3**). As such, the PARAFAC models of plaque microbiomes describe microbial subcommunities with common dynamics that connect to the magnitude of the gingivitis response.

We further investigated the robustness of the ecosystem during gingivitis onset and progression by comparing the sum of the relative abundances of clustered ASVs at the start and end of the intervention (**Supplementary Table B3**). We found significant differences between the relative abundances of some ASV clusters at the start and end of the gingivitis challenge in lower jaw lingual (ASV cluster 1) and upper jaw interproximal (ASV cluster 4) plaque microbiomes in all response groups (Benjamini-Hochberg corrected two-sided Wilcoxon rank sum test: $p \leq 7.2e-13$ and $p \leq 2.6e-$

148 6, respectively). For a further three ASV clusters (upper jaw lingual ASV cluster 1 and upper jaw
149 interproximal clusters 1 and 3), we found the sum of relative abundances to be significantly different
150 (p=0.002, p=0.0025, p=0.0039, respectively) in high responders, but not in low responders. These
151 results suggest that ecosystem stability is different between high and low responders in several oral
152 niches.

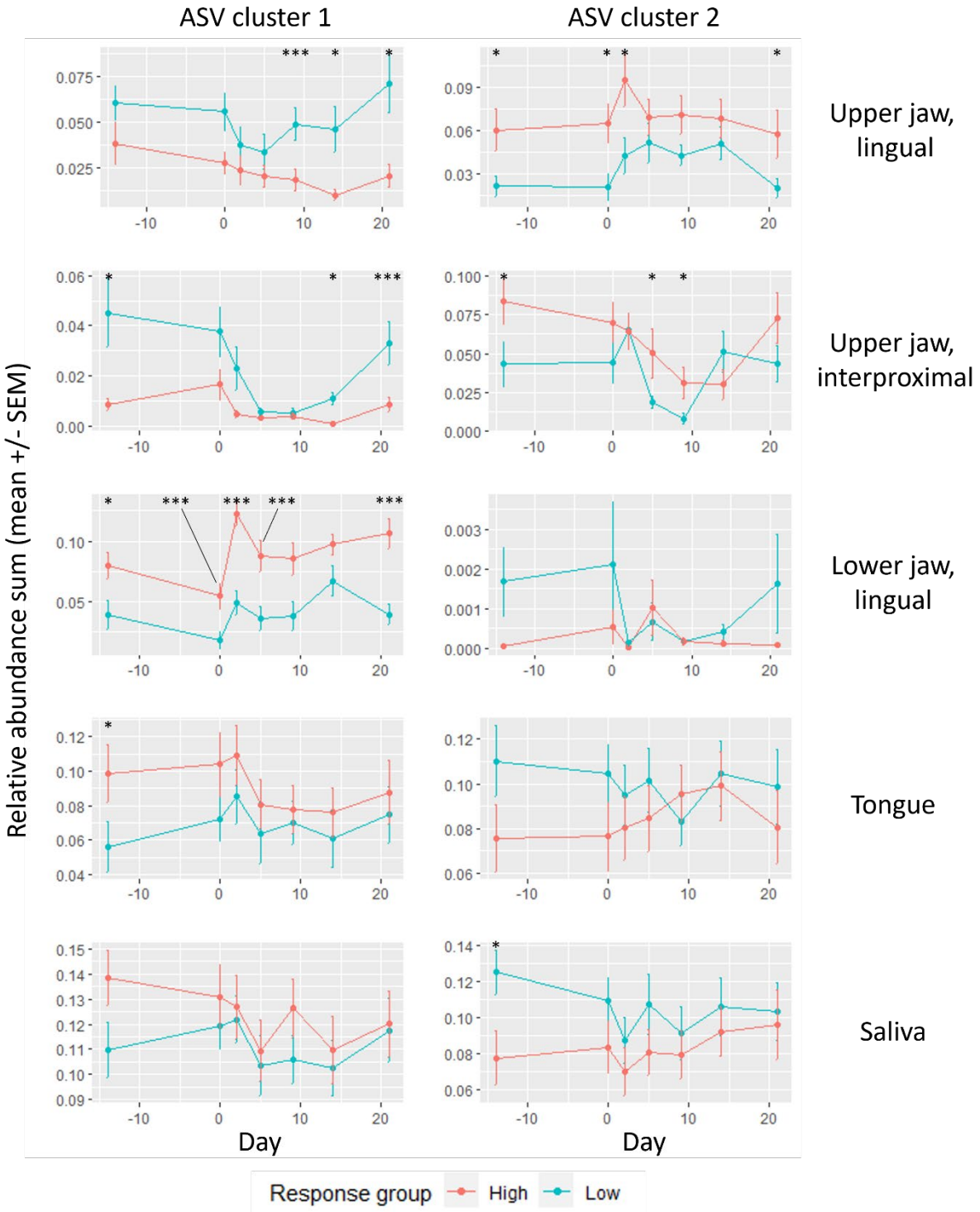

Figure 3: Overview of the sums of relative abundances per ASV cluster and sample type, separating subjects by response group. Error bars correspond to the standard error of the mean (SEM). The mean difference between the high and low response groups per time point was tested using a Benjamini-Hochberg corrected permutation test of 999 iterations (: p≤0.05; **: p≤0.01; ***: p≤0.001). Mid responders and ASV clusters 3 and 4 of the upper jaw interproximal plaque samples are not shown for visual clarity (**Supplementary Figure A3** and **A4**, respectively). Please refer to **Table 2** for the list of identified species per ASV cluster.*

161 *Integration of the microbiome and metabolome PARAFAC models identifies host-microbiome*
162 *interactions at the pathway level*

163 With the established connection between the clinical parameters of gingivitis and the variation in
164 the plaque microbiomes as modelled by PARAFAC, we investigated host-microbiome interactions
165 at the biochemical pathway level. We obtained functional predictions of the microbiome per oral
166 site using Tax4Fun2[34,35]. We then created separate PARAFAC models of the salivary metabolomics
167 data and of the functional prediction of the microbiomes at each oral site. Despite correcting for
168 correlation between most salivary metabolite levels, likely due to variable water content of the
169 saliva (see Methods), the subject loadings of both components of the model corresponding to the
170 salivary metabolome were found to correlate with the correcting factor ($p=2.0e-14$ and $p=2.0e-5$,
171 respectively). Regardless, we expected the salivary metabolomics model to have sufficient freedom
172 to also describe variation related to the gingivitis response.

173 The well-modelled molecular functions (KEGG orthologous groups belonging to pathways that
174 produce or consume the salivary metabolites) and well-modelled salivary metabolites were
175 combined in a ranked list. KEGG-pathway enrichment was identified using SetRank, which is a
176 functional enrichment algorithm that corrects for multiple pathway membership[36]. This revealed
177 that the microbiome and metabolome responses to the gingivitis challenge reflected differences in
178 carbon and energy metabolism, as well as cell wall structure (**Figure 4, Supplementary Figure A5,**
179 **Supplementary Table B4**). For example, the tongue microbiome and salivary metabolome were
180 involved in a joint response in the biosynthesis of cofactors and carbon metabolism ($p=0.0045$ and
181 $p=0.0052$, respectively). The quorum sensing pathway was significantly enriched in all plaque
182 microbiomes ($p \leq 0.05$). The pathway enrichment results therefore reflect the microbiome responses
183 and highlight potential metabolic interactions with the human host.

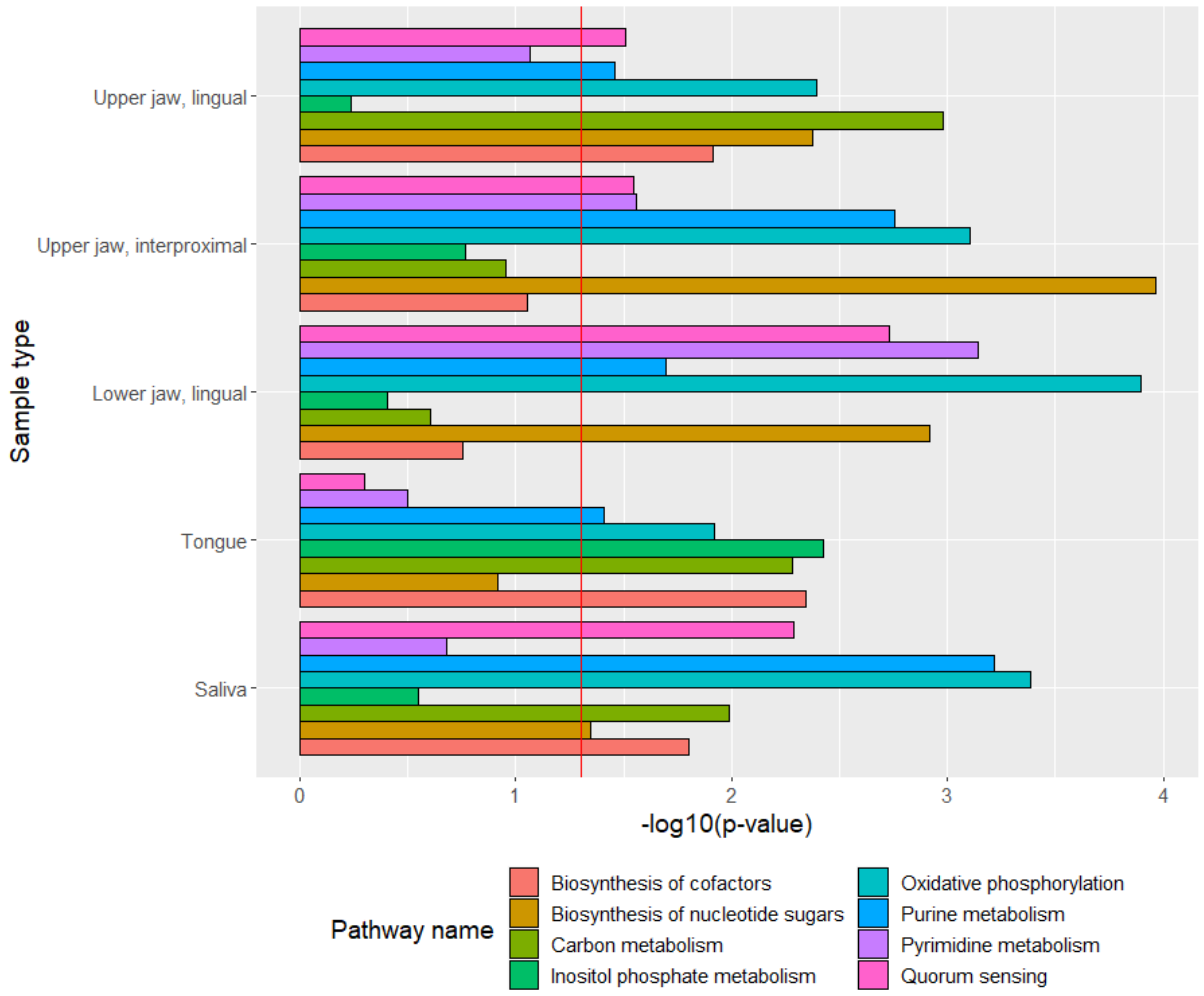

Figure 4: Overview of the pathway enrichment results per combination of oral site microbiome and the salivary metabolome. Tax4Fun2 was used to create functional predictions from ASV data. Well-modelled metabolites and microbiome molecular functions were integrated by mapping them to KEGG pathway level. SetRank was then used to test for pathway enrichment and corrected for multiple-pathway membership. Pathways were filtered to be significant (p<=0.01) in at least one sample type and to contain at least two well-modelled KEGG molecular functions and two well-modelled metabolites. The red vertical line corresponds to p=0.05.

Discussion

We have shown that the unsupervised modelling approach of PARAFAC mainly described variation between subjects, as expected from an algorithm describing the maximum amount of variation that is present in the data. The modelled variation could be attributed to clinically relevant parameters. In addition, we have observed that the model corresponding to the salivary metabolomics samples partly describes the salivary dilution despite correcting for it using Probabilistic Quotient Normalization[37]. This might be an artifact due to an incorrect assumption that correcting for water content of saliva can be done in the same way as for urine metabolomics samples. Future work on this topic should focus on the appropriateness of using Probabilistic Quotient Normalization prior to performing a decomposition analysis. Other multi-way approaches exist to describe a specific type of variation[28–30]. For example, in N-way partial least squares (NPLS) the model is constrained to regress on an outcome variable[38]. Additionally, the PARAFAC models of the microbiome and metabolome could be created in a linked fashion by keeping one of the modes equal to each other, known as coupled matrix and tensor factorization[39–41]. Each of these approaches might yield new insights as the models explicitly look at variation that is common between the datasets. Further research is needed to compare such methods to PARAFAC in the context of multi-omics data.

We observed that the microbiome PARAFAC models partly describe richness and evenness. This result gives further evidence of a relationship between oral health and microbial diversity which has been described before[42–44]. We identified several microbial subcommunities within the oral sites that responded similarly to the intervention, for example a group of ASVs that was significantly more abundant in individuals in the high responder group compared to low responders, which represented species of known pathogenic or pro-inflammatory genera such as *Actinomyces*, *Campylobacter*, *Capnocytophaga*, *Fusobacterium*, *Leptotrichia*, and *Porphyromonas*[5,19,20,45,46]. Clusters of ASVs that were significantly more abundant in low responders compared to high responders consisted of known commensal species related to oral health, such as *Kingella oralis*[47], *Streptococcus* spp.[48,49], and *Veillonella* spp.[50]. Finally, we observed a difference in ecosystem stability between high and low responders in some parts of the oral cavity. This suggests that in some subjects, the ecosystem can withstand the ecological pressure of plaque accumulation and has some mechanisms that prevents healthy microbiota from decreasing in abundance. Further research is needed to identify these mechanisms and the microbiota involved.

222 By integrating the PARAFAC models of the salivary metabolomics data and of the predicted
223 metabolic functions from the microbiome data, we identified enriched pathways that reflected the
224 changing proportions of Gram-positive and -negative microbiota (cell membrane/wall component
225 pathways, such as lipopolysaccharide and peptidoglycan biosynthesis). Quorum sensing systems
226 were found to be significantly enriched in all plaque sites likely due to the variation in *Streptococcus*
227 spp. and their genes for oligopeptide binding protein quorum sensing system[51,52]. These are known
228 to regulate biofilm formation and virulence[53–55]. The observed significance of the non-mevalonate
229 pathway of isopentenyl pyrophosphate and dimethylallyl pyrophosphate in the upper jaw
230 interproximal plaque was likely related to the same variation[56]. The strong signal in carbon
231 metabolism and oxidative phosphorylation were likely reflective of the variation in anaerobic
232 bacteria, which accumulate during gingivitis[21,57,58]. An interesting link between salivary metabolites
233 and microbiome functional potential may have been observed in the nucleoside/purine/pyrimidine
234 biosynthesis pathways: while urea was one of the best modelled salivary metabolites and is a
235 potential biomarker for oral health[59–62], a role of salivary nucleosides in plaque formation or
236 gingivitis is as yet unknown.

237 In conclusion, we show that PARAFAC modelling of longitudinal oral microbiome and salivary
238 metabolomics data can be used to identify clinically relevant variation and similarly responding
239 microbial subcommunities related to gingivitis. By performing high level integration of predicted
240 microbiome functions and the salivary metabolome, we highlight biochemical pathways of oral
241 biofilm formation and maturation with a likely role in gingivitis.

242 Methods

243 *Data description*

244 The gingivitis challenge study was carried out at the Academic Centre for Dentistry Amsterdam
245 (ACTA) with 15 systemically healthy males and 26 systemically healthy females between the ages
246 of 18 and 55. Recruitment details and exclusion criteria were previously described[27]. Reversible
247 gingivitis was induced by omission of oral hygiene during the two-week gingivitis challenge (day 0
248 to day 14), which was preceded by a two-week baseline period (day -14 to day 0) and followed by a
249 one-week resolution phase (day 14 to day 21; **Figure 1A**). Assessment of plaque formation, bleeding
250 and the collection of oral samples for microbiome were performed throughout the baseline,
251 challenge and resolution phases. Oral samples for microbiome analysis were taken at six sites in the
252 mouth: supragingival plaque at the lower and upper jaw lingual surfaces, supragingival plaque at the

253 lower and upper jaw interproximal surfaces, tongue and saliva. The salivary metabolome was only
254 sampled during the challenge phase.

255 *Red fluorescence imaging*

256 Acquisition of red fluorescent plaque (RF) photographs has been described previously[18,63,64]. Briefly,
257 fluorescence photographs were taken of the vestibular aspect of the anterior teeth (cuspid to cuspid,
258 upper and lower jaw) in end-to-end position at every time point using a QLF-D camera (Inspektor
259 Research Systems BV, Amsterdam, the Netherlands). The photographs were assessed
260 planimetrically for the percentage red fluorescent protein (RFP) coverage using RFP analysis
261 software (QA2 V1.25, Inspektor Research Systems BV, Amsterdam, the Netherlands). Three
262 response groups were determined using the RF% values on day 14: low (0-1.7%), mid (1.8-6.0%)
263 and high (6.0%+)[18] (**Figure 1C**).

264 *DNA isolation and 16S rRNA gene amplicon sequencing*

265 DNA was isolated from the samples using a previously described method[65]. Samples were mixed
266 with 300 µl lysis buffer (Agowa, Berlin, Germany), 500 µl phenol saturated with tris-HCl (pH 8.0)
267 and 500 µl zirconium beads (0.1 mm; BioSpec Products, Bartlesville, OK, USA), and shaken in a bead
268 beater for 3 min at 2800 oscillations/min. DNA released was purified using magnetic beads (Agowa,
269 Berlin, Germany) and used for amplicon sequencing.

270 The V4 hypervariable region of the 16S rRNA gene was targeted using primers F515 (5'- GTG CCA
271 GCM GCC GCG GTA A -3') and R806 (5'- GGA CTA CHV GGG TWT CTA AT -3'). The primers
272 included Illumina adapters and a unique 8-nucleotide sample index sequence key[66]. PCR was
273 performed using the Phusion Hot Start II High Fidelity PCR Master Mix (Thermo Scientific,
274 Waltham, MA, USA) with 100 pg template. The following amplification program was used: initial
275 denaturation at 98°C for 30 s; 30 cycles of 98°C for 10 s, 55°C for 30 s and 72°C for 30 s; and final
276 elongation at 72°C for 5 min. The amplicon libraries were pooled in equimolar amounts and purified
277 using the QIAquick Gel Extraction Kit (Qiagen, Valencia, CA, USA). Amplicon quality and size
278 were analysed on a Fragment Analyzer (Advanced Analytical Technologies Inc., Ankeny, IA, USA).
279 Amplicon sequencing was performed on the Illumina MiSeq platform (Illumina Technologies, San
280 Diego, CA, USA) using 2 x 200 cycle paired-end settings.

281 *16S rRNA gene data pre-processing*

282 The 16S rRNA gene sequencing data were pre-processed using DADA2[67] (version 1.14.0). All
283 microbiome sampling locations except for saliva were pre-processed with default DADA2 settings
284 (truncLen = c(100, 100), maxN = 0, maxEE = c(2,2), tuncQ = 2, rm.phix = TRUE, compress = FALSE,
285 matchIDs = TRUE, multithread = TRUE). The saliva samples were processed with a shorter
286 trimming setting (truncLen = c(200, 215)) due to lower quality reads. Taxonomic classification of
287 ASVs was performed using the SILVA (v138) and HOMD (v15.22) reference databases.

288 *Metabolomics sampling and profiling*

289 Saliva sample collection and metabolite profiling were described previously[27]. Unstimulated saliva
290 was collected at the intervention time points. Participants were instructed to allow saliva to
291 accumulate on the floor of the mouth and to spit at 30 second intervals into a pre-weighted 30 ml
292 polypropylene tube. The collection period was 5 minutes. Non-targeted metabolite profiling of the
293 saliva samples for the gingivitis challenge time points was performed by Metabolon. Samples were
294 processed as described in Metabolon's standard method[68]. Raw data were extracted, peak-identified
295 and quality controlled using Metabolon's hardware and software. Compounds were identified by
296 comparison with Metabolon's reference library[69]. Metabolites were annotated with KEGG
297 compound IDs[70,71].

298 *Assessment of clinical parameters of gingivitis*

299 Plaque and bleeding scores were clinically assessed by two experts in a half mouth randomized
300 contralateral model, as described previously[18]. Plaque was quantified using a modified Silness & Loë
301 Plaque Index at six sites of the buccal and lingual aspects of all present teeth[72]. Gingival bleeding
302 was quantified using the bleeding on marginal probing index on six gingival areas on the buccal and
303 lingual sides of all present teeth[73].

304 *Statistical Analysis*

305 *Microbiome data processing*

306 The ASV data and taxonomic information were processed using MATLAB (version 2022a). The data
307 were separated by oral site. To limit the sparsity per dataset, ASVs were kept if the sparsity was
308 <50% in any response group (**Supplementary Figure A6**). All other ASVs were removed from the
309 data. By setting a response group-based sparsity-cutoff per ASV, we avoid removing biologically
310 relevant ASVs that would occur in only one or two response groups. ASVs were also removed if

311 they corresponded to chloroplast or mitochondrial sequences, as these were not relevant for the
312 study. An overview of the number of ASVs before and after filtering per sample type is reported in
313 **Supplementary Table B5**. Subsequently, a centred-log ratio transformation - using a pseudo-count
314 of 1 - was performed to correct for compositionality[74,75]. The datasets were then converted to three-
315 way arrays (**Figure 1D**). Missing samples were kept in the data cube as a row of missing values
316 (**Supplementary Table B6**). This is possible because PARAFAC interpolates the missing data
317 automatically in its alternating least-squares algorithm and maximises the amount of information
318 for the modelling procedure as the other samples of the subject do not have to be removed entirely.
319 Subsequently, centring across the subject mode and scaling within the ASV mode - ignoring missing
320 values - was performed to make the samples comparable at every timepoint and the ASVs
321 comparable for all time points[76].

322 *Salivary metabolomics data processing*

323 The salivary metabolomics data were processed using MATLAB (version 2022a). To limit the
324 sparsity per dataset, metabolites were excluded if they contained more than 25% values below the
325 detection limit (**Supplementary Figure A7**). Additionally, xenobiotic compounds were manually
326 assessed for occurrence across response groups and selected if they were prevalent in most subjects
327 (**Supplementary Data**). After feature selection, 400 of the 499 metabolites remained (**Supplementary**
328 **Table B5**). Values below the detection limit were imputed with a random value between 0 and the
329 detection limit per metabolite to preserve their distribution. To correct for the dilution caused by
330 the amount of water in the saliva samples, Probabilistic Quotient Normalization (PQN) was
331 performed using the median value of each metabolite as an artificial reference sample[37]. Next, the
332 dataset was (natural) log transformed to stabilize the variance. The dataset was then converted to a
333 three-way array. Subsequently, centring across the subject mode and scaling within the ASV mode
334 - ignoring missing values - was performed to make the samples comparable at every timepoint and
335 the ASVs comparable for all time points[76]. All subjects were fully sampled, except for subject
336 3CN8CB for whom no metabolome data was available (**Supplementary Table B6**).

337 *Functional profile prediction of microbiome data*

338 A functional profile prediction based on the microbiome ASV count data was performed using the
339 Tax4Fun2 package[34,35] in R (Tax4Fun2 version 1.1.5, R version 4.0.3). ASVs corresponding to
340 Chloroplast or Mitochondria were removed. Samples were rarefied to 10 000 reads to make them

341 comparable (**Supplementary Figures A8** and **A9**). Samples with fewer total reads were removed. This
342 step removed 53 of 1 692 samples. ASVs without counts after rarefying were removed. All steps
343 together removed 6 903 out of 14 014 ASVs. Tax4Fun2 was run with default settings against the
344 included Ref99NR database[35] and a custom database based on the HOMD genomes[77] (v9.14, accessed
345 2020-11-09). Molecular functions of the genomes were assigned using Tax4Fun2's DIAMOND
346 wrapper[78]. HOMD-annotated 16S rRNA gene sequences were extracted from the genomes, cut to
347 the 515F-806R fragment used in this study using cutadapt[79] v1.18. Exact duplication within genomes
348 were removed, and 16S rRNA gene sequence fragments were combined with the functional
349 assignments using Tax4Fun's generateUserDataByClustering function. The resulting functional
350 prediction profiles - which contain values between 0 and 1 for each function - were used for
351 subsequent analysis. The fraction of unused taxonomic units and the fraction of unused sequences
352 are reported per sample (**Supplementary Figures A10** and **A11**).

353 *Processing of functional profile predictions*

354 The functionally predicted microbiome data were processed in MATLAB (version 2022a). The data
355 were separated by sample type. To make the data comparable to the salivary metabolomics data,
356 predicted KEGG orthologous groups (KOs) were removed if they did not belong to pathways that
357 the metabolites mapped to. This was done by mapping the KOs and metabolite compound IDs to
358 pathways using the KEGG API[80]. To limit the sparsity per dataset, KOs were removed if the number
359 of zeroes for all response groups was >50% (**Supplementary Figure A12**). Additionally, KOs were
360 removed if the sum-of-squares was lower than 0.025% of the total sum-of-squares of the dataset
361 (**Supplementary Figure A13**). This latter filter was to ensure that the modelling procedure focused
362 on relevant variation in the data and made the total number of variables comparable to the
363 metabolomics data, while retaining most information. An overview of the number of KOs remaining
364 after feature selection is reported (**Supplementary Table B5**). Subsequently a centred-log ratio
365 transformation of each dataset was performed to correct for compositionality[74,75]. The dataset was
366 then converted to a three-way array. Missing samples were kept in the data cube as a row of missing
367 values (**Supplementary Table B6**). Subsequently, centring across the subject mode and scaling within
368 the ASV mode - ignoring missing values - was performed to make the samples comparable at every
369 timepoint and the ASVs comparable for all time points[76].

370 *Parallel Factor Analysis (PARAFAC)*

371 Details on the creation of PARAFAC models for microbiome[81] and metabolomics data[30] have been
372 described elsewhere. The PARAFAC implementation from the N-way toolbox[82] (version 1.8.0.0) in
373 Matlab (version 2022a) was used to create PARAFAC models for all datasets. Similar to PCA, the
374 correct number of components of the PARAFAC model needed to be determined to create an
375 optimal model[31]. This was done by inspecting the number of iterations needed to converge [30], the
376 core consistency diagnostic[31], the variation explained[30], and the Tucker congruence coefficient per
377 mode[32,33]. Additionally, a jack-knife approach was used to determine the stability of the PARAFAC
378 modelling procedure. These metrics were inspected per component for every generated model
379 (**Supplementary Data**). All generated models are reported in **Supplementary Figures A14-A26**. An
380 overview of the model statistics also reported (**Supplementary Table B7**). Congruence loadings,
381 which describe the relationships between the original variables of the dataset and the latent
382 variables of the corresponding model, were calculated for every component in every sample type[83].

383 A transformation of the subject loadings was required for comparison with the longitudinally
384 measured clinical parameters of gingivitis. The ASV loading vectors were orthonormalized using
385 the Gram-Schmidt orthonormalization procedure in the pracma[84,85] R package (version 2.4.2). The
386 (same) transformation matrix is then applied to the Kronecker product of the subject and the time
387 loadings to obtain interpretable loadings of every subject-time combination[86]. The correlation of the
388 time-resolved subject loadings with the clinical parameters of gingivitis was then tested (**Table 1**
389 and **Supplementary Table B1**).

390 *Microbiome ASV clustering*

391 Loading plots of the ASV mode and the subject mode for each of the microbiome PARAFAC models
392 were created (**Figure 2**). ASVs were filtered out if they had a variation explained lower than the
393 average of the model or a congruence loading lower than 0.4[83]. ASVs were clustered based on their
394 fitted abundances according to the PARAFAC model using the K-medoids algorithm from the
395 cluster R package[87] (version 2.1.4) with 50 random starts to be robust against outliers. The number
396 of clusters was determined using the within-cluster sum of squares, silhouette width and gap statistic
397 metrics as reported by the factoextra R package[88] (version 1.0.7, **Supplementary Figure A27**). An
398 overview of the taxonomic information per cluster can be found in **Table 2**.

399 The response to the gingivitis intervention of the ASV clusters was shown using the relative
400 abundance sum per ASV cluster derived from the original count data (**Figure 3** and **Supplementary**

401 **Figure A3**). The mean of the summed relative abundances and standard error of the mean were
402 calculated per response group for a given sample type and time point. The mean difference between
403 the high and low responders was tested using a permutation analysis where the response group
404 membership of the subjects was permuted (**Supplementary Table B2**).

405 *Functional enrichment analysis*

406 The PARAFAC models of the functionally profiled microbiome and salivary metabolomics data
407 were combined to perform a pathway enrichment test per sample type. This was done by calculating
408 the variance explained and congruence loadings per KO or metabolite in each model[83]. If the
409 PARAFAC model contained two components, the maximum of the two congruence loadings per
410 feature was used. The variance explained and congruences were normalized by the maximum value
411 per model prior to integration. The normalized variance explained and normalized congruence per
412 feature were averaged to obtain a ranking of pathway elements (KOs and metabolites). This causes
413 the best modelled KO and compound ID to be at the top of this list. The ranked pathway element
414 list was cut off at 75% of its length to ensure a good separation between well-modelled and
415 averagely-modelled pathway elements (**Supplementary Figure A28**).

416 The SetRank R package (version 1.1.0) was used to obtain pathways of interest[36]. SetRank is a gene
417 set enrichment algorithm that obtains a high sensitivity by correcting for multiple pathway
418 membership. A custom database of pathway elements was created by combining the KO and
419 compound ID to pathway mappings obtained through the KEGG API (**Supplementary Data**).
420 Pathways were removed from our database if they could not be performed by prokaryotes. Generic,
421 large pathways with more than 750 elements were removed to ensure that the enrichment results
422 were specific enough for interpretation (**Supplementary Figure A29**). Subsequently the SetRank
423 analysis was performed with standard settings per sample type. The multiple-pathway corrected p-
424 values are reported ($p \leq 0.05$, **Figure 4** and **Supplementary Table B4**)

425 Data Availability

426 The datasets [GENERATED/ANALYZED] for this study can be found in the European Genome-phenome
427 Archive (EGA; https://ega-archive.org).

428 Code Availability

429 The underlying code for this study is available on GitHub and can be accessed via this link
430 https://zenodo.org/doi/10.5281/zenodo.10450355

Ethics statement

The study involving human participants was conducted in accordance with the ethical principles of the 64th WMA Declaration of Helsinki (October 2013, Brazil) and the Medical Research Involving Human Subjects Act (WMO), approximating Good clinical Practice (CPMP/ICH/135/95) guidelines. The clinical trial was approved by the Medical Ethical Committee of the VU Medical Center (2014.505) and registered at the public trial register of the Central Committee on Research Involving Human Subjects (CCMO) under number NL51111.029.14.

Author Contributions

G.R. van der Ploeg: formal analysis, methodology, writing - original draft; B.W. Brandt: investigation, writing - review & editing; B.J.F. Keijser: investigation, project administration, writing - review & editing; M.H. van der Veen: investigation, project administration, writing - review & editing; C.M.C. Volgenant: investigation, writing - review & editing; E. Zaura: conceptualization, investigation, project administration, funding acquisition, writing - review & editing; A.K. Smilde: conceptualization, methodology, supervision, funding acquisition, writing - review & editing; J.A. Westerhuis: conceptualization, methodology, supervision, formal analysis, writing - original draft; A. Heintz-Buschart: conceptualization, formal analysis, supervision, project administration, writing - original draft. All authors reviewed and approved the manuscript.

Competing interests

The authors declare that the research was conducted in the absence of any commercial or financial relationships that could be construed as a potential conflict of interest.

Acknowledgements

We want to thank Michelle van der Wurff (TNO) and Tim van den Broek (TNO) for their help in data acquisition, processing and storing and Jesse Alderliesten (UU/UvA), Fred White (UvA), Cynthia Albracht (UvA), Juan Pablo Bascur (CWTS) and Rianne Warmerdam (Aiden) for their useful discussions and suggestions. The authors thank N.A.M. Rosema for coordinating the clinical study. For assistance in capturing fluorescence photographs, the authors thank Y. Altindağ. For the clinical examinations the authors thank J.M. Voll (clinical plaque assessment with Silness & Löe), and S. Bizzarro (assessment of the bleeding on marginal probing).

This research is supported by the Dutch Technology Foundation STW (project number 10948) and the Top Institute Food and Nutrition (TIFN), a public-private partnership on precompetitive research in food and nutrition. Organizations supporting this project had no role in study design, data collection

462 and analysis, decision to publish, or preparation of the manuscript. QLF data was obtained with funding
463 from NOW (ZonMw-STW-NIG-program): "Project 10948: Seeing is believing? A novel tool for the
464 visualization of oral disease manifestations." GRvdP was funded by a grant from the University of
465 Amsterdam, Research Priority Area on Personal Microbiome Health.

466

467 ## References

468 1. Petersen, P. E., Bourgeois, D., Ogawa, H., Estupinan-Day, S. & Ndiaye, C. The global burden of oral
469 diseases and risks to oral health. *Bull. World Health Organ.* (2005).
470 2. Peres, M. A. *et al.* Oral diseases: a global public health challenge. *The Lancet* **394**, 249–260 (2019).
471 3. WHO. *Global oral health status report: towards universal health coverage for oral health by 2030*.
472 https://www.who.int/publications/i/item/9789240061484 (2022).
473 4. Widström, E., Eaton, K. & Vanobbergen, J. Oral healthcare systems in the Extended European
474 Union, partim:[Oral Health care system in] Belgium. *Oral Health Prev. Dent.* **2**, 155–157 (2004).
475 5. Huang, S. *et al.* Predictive modeling of gingivitis severity and susceptibility via oral microbiota.
476 *ISME J.* **8**, 1768–1780 (2014).
477 6. Chapple, I. L. C. *et al.* Primary prevention of periodontitis: managing gingivitis. *J. Clin. Periodontol.*
478 **42**, S71–S76 (2015).
479 7. Curtis, M. A., Diaz, P. I. & Van Dyke, T. E. The role of the microbiota in periodontal disease.
480 *Periodontol. 2000* **83**, 14–25 (2020).
481 8. Löe, H., Theilade, E. & Jensen, S. B. Experimental Gingivitis in Man. *J. Periodontol.* **36**, 177–187
482 (1965).
483 9. Murakami, S., Mealey, B. L., Mariotti, A. & Chapple, I. L. C. Dental plaque–induced gingival
484 conditions. *J. Clin. Periodontol.* **45**, S17–S27 (2018).
485 10. Han, L. *et al.* Hygiene practices among young adolescents aged 12-15 years in low- and middle-
486 income countries: a population-based study. *J. Glob. Health* **10**, 020436 (2020).

487 11. Chapple, I. L. C. *et al.* Periodontal health and gingival diseases and conditions on an intact and a
488 reduced periodontium: Consensus report of workgroup 1 of the 2017 World Workshop on the
489 Classification of Periodontal and Peri-Implant Diseases and Conditions. *J. Periodontol.* **89**, S74–S84
490 (2018).
491 12. Kilian, M. *et al.* The oral microbiome – an update for oral healthcare professionals. *Br. Dent. J.* **221**,
492 657–666 (2016).
493 13. Van Der Velden, U., Kuzmanova, D. & Chapple, I. L. C. Micronutritional approaches to periodontal
494 therapy. *J. Clin. Periodontol.* **38**, 142–158 (2011).
495 14. Bergström, J. & Preber, H. The influence of cigarette smoking on the development of experimental
496 gingivitis. *J. Periodontal Res.* **21**, 668–676 (1986).
497 15. Nibali, L., Di Iorio, A., Tu, Y. & Vieira, A. R. Host genetics role in the pathogenesis of periodontal
498 disease and caries. *J. Clin. Periodontol.* **44**, (2017).
499 16. Axelsson, P., Lindhe, J. & Nyström, B. On the prevention of caries and periodontal disease. *J. Clin.*
500 *Periodontol.* **18**, 182–189 (1991).
501 17. Guk, H.-J., Lee, E.-S., Jung, U.-W. & Kim, B.-I. Red fluorescence of Interdental plaque for screening
502 of gingival health. *Photodiagnosis Photodyn. Ther.* **29**, 101636 (2020).
503 18. van der Veen, M. H., Volgenant, C. M. C., Keijser, B., ten Cate, J. (Bob) M. & Crielaard, W. Dynamics
504 of red fluorescent dental plaque during experimental gingivitis—A cohort study. *J. Dent.* **48**, 71–
505 76 (2016).
506 19. Kistler, J. O., Booth, V., Bradshaw, D. J. & Wade, W. G. Bacterial Community Development in
507 Experimental Gingivitis. *PLoS ONE* **8**, e71227 (2013).
508 20. Schincaglia, G. P. *et al.* Clinical, Immune, and Microbiome Traits of Gingivitis and Peri-implant
509 Mucositis. *J. Dent. Res.* **96**, 47–55 (2017).
510 21. Diaz, P. I., Zilm, P. S. & Rogers, A. H. Fusobacterium nucleatum supports the growth of
511 Porphyromonas gingivalis in oxygenated and carbon-dioxide-depleted environments.
512 *Microbiology* **148**, 467–472 (2002).

513 22. Ter Steeg, P. F., Van Der Hoeven, J. S., De Jong, M. H., Van Munster, P. J. J. & Jansen, M. J. H.
514 Modelling the Gingival Pocket by Enrichment of Subgingival Microflora in Human Serum in
515 Chemostats. *Microb. Ecol. Health Dis.* **1**, 73–84 (1988).
516 23. Dawes, C. & Wong, D. T. W. Role of Saliva and Salivary Diagnostics in the Advancement of Oral
517 Health. *J. Dent. Res.* **98**, 133–141 (2019).
518 24. Proctor, G. B. The physiology of salivary secretion. *Periodontol. 2000* **70**, 11–25 (2016).
519 25. König, K. G. & Navia, J. M. Nutritional role of sugars in oral health. *Am. J. Clin. Nutr.* **62**, 275S-282S
520 (1995).
521 26. Marsh, P. D. Sugar, fluoride, pH and microbial homeostasis in dental plaque. *Proc. Finn. Dent. Soc.*
522 *Suom. Hammaslaakariseuran Toim.* **87**, 515–525 (1991).
523 27. Prodan, A. *et al.* Effect of experimental gingivitis induction and erythritol on the salivary
524 metabolome and functional biochemistry of systemically healthy young adults. *Metabolomics* **12**,
525 147 (2016).
526 28. Carroll, J. D. & Chang, J.-J. Analysis of individual differences in multidimensional scaling via an n-
527 way generalization of “Eckart-Young” decomposition. *Psychometrika* **35**, 283–319 (1970).
528 29. Harshman, R. A. Foundations of the PARAFAC procedure: Models and conditions for an"
529 explanatory" multimodal factor analysis. (1970).
530 30. Bro, R. PARAFAC. Tutorial and applications. *Chemom. Intell. Lab. Syst.* (1997).
531 31. Bro, R. & Kiers, H. A new Efficient Method for Determining the Number of Components in PARAFAC
532 Models. *J. Chemom.* **17**, 274–286 (2003).
533 32. Lorenzo-Seva, U. & ten Berge, J. M. F. Tucker’s congruence coefficient as a meaningful index of
534 factor similarity. *Methodol. Eur. J. Res. Methods Behav. Soc. Sci.* **2**, 57–64 (2006).
535 33. Tucker, L. R. *A method for synthesis of factor analysis studies*. vol. 984 (Educational Testing Service
536 Princeton, NJ, 1951).
537 34. Aßhauer, K. P., Wemheuer, B., Daniel, R. & Meinicke, P. Tax4Fun: predicting functional profiles
538 from metagenomic 16S rRNA data. *Bioinformatics* **31**, 2882–2884 (2015).

539 35. Wemheuer, F. *et al.* Tax4Fun2: prediction of habitat-specific functional profiles and functional
540 redundancy based on 16S rRNA gene sequences. *Environ. Microbiome* **15**, 11 (2020).
541 36. Simillion, C., Liechti, R., Lischer, H. E. L., Ioannidis, V. & Bruggmann, R. Avoiding the pitfalls of gene
542 set enrichment analysis with SetRank. *BMC Bioinformatics* **18**, 151 (2017).
543 37. Dieterle, F., Ross, A., Schlotterbeck, G. & Senn, H. Probabilistic Quotient Normalization as Robust
544 Method to Account for Dilution of Complex Biological Mixtures. Application in 1H NMR
545 Metabonomics. *Anal. Chem.* **78**, 4281–4290 (2006).
546 38. Bro, R. Multiway calibration. Multilinear PLS. *J. Chemom.* **10**, 47–61 (1996).
547 39. Acar, E. *et al.* Structure-revealing data fusion. *BMC Bioinformatics* **15**, 239 (2014).
548 40. Acar, E., Bro, R. & Smilde, A. Data Fusion in Metabolomics Using Coupled Matrix and Tensor
549 Factorizations. *Proc. IEEE* **103**, 1602 (2015).
550 41. Singh, A. P. & Gordon, G. J. Relational learning via collective matrix factorization. in *Proceedings of*
551 *the 14th ACM SIGKDD international conference on Knowledge discovery and data mining* 650–658
552 (Association for Computing Machinery, 2008). doi:10.1145/1401890.1401969.
553 42. Anderson, A. C. *et al.* In-vivo shift of the microbiota in oral biofilm in response to frequent sucrose
554 consumption. *Sci. Rep.* **8**, 14202 (2018).
555 43. Schoilew, K. *et al.* Bacterial biofilm composition in healthy subjects with and without caries
556 experience. *J. Oral Microbiol.* **11**, 1633194 (2019).
557 44. Thomas, A. M. *et al.* Alcohol and tobacco consumption affects bacterial richness in oral cavity
558 mucosa biofilms. *BMC Microbiol.* **14**, 250 (2014).
559 45. Kirst, M. E. *et al.* Dysbiosis and Alterations in Predicted Functions of the Subgingival Microbiome
560 in Chronic Periodontitis. *Appl. Environ. Microbiol.* **81**, 783–793 (2015).
561 46. The Human Microbiome Project Consortium. Structure, function and diversity of the healthy
562 human microbiome. *Nature* **486**, 207–214 (2012).
563 47. Abusleme, L., Hoare, A., Hong, B. & Diaz, P. I. Microbial signatures of health, gingivitis, and
564 periodontitis. *Periodontol. 2000* **86**, 57–78 (2021).

565 48. Caporaso, J. G. *et al.* Moving pictures of the human microbiome. *Genome Biol.* **12**, R50 (2011).

566 49. Zaura, E., Keijser, B. J., Huse, S. M. & Crielaard, W. Defining the healthy" core microbiome" of oral
567 microbial communities. *BMC Microbiol.* **9**, (2009).

568 50. Moore, W. E. C. & Moore, L. V. H. The bacteria of periodontal diseases. *Periodontol. 2000* **5**, 66–
569 77 (1994).

570 51. Fontaine, L. *et al.* A Novel Pheromone Quorum-Sensing System Controls the Development of
571 Natural Competence in *Streptococcus thermophilus* and *Streptococcus salivarius*. *J. Bacteriol.* **192**,
572 1444–1454 (2010).

573 52. Gardan, R., Besset, C., Guillot, A., Gitton, C. & Monnet, V. The Oligopeptide Transport System Is
574 Essential for the Development of Natural Competence in *Streptococcus thermophilus* Strain LMD-
575 9. *J. Bacteriol.* **191**, 4647–4655 (2009).

576 53. Hammer, B. K. & Bassler, B. L. Quorum sensing controls biofilm formation in *Vibrio cholerae*. *Mol.*
577 *Microbiol.* **50**, 101–104 (2003).

578 54. Kong, K.-F., Vuong, C. & Otto, M. Staphylococcus quorum sensing in biofilm formation and
579 infection. *Int. J. Med. Microbiol.* **296**, 133–139 (2006).

580 55. Preda, V. G. & Săndulescu, O. Communication is the key: biofilms, quorum sensing, formation and
581 prevention. *Discoveries* **7**, (2019).

582 56. Odom, A. R. Five questions about non-mevalonate isoprenoid biosynthesis. *PLoS Pathog.* **7**,
583 e1002323 (2011).

584 57. Chen, M. *et al.* Oxidative stress-related biomarkers in saliva and gingival crevicular fluid associated
585 with chronic periodontitis: A systematic review and meta-analysis. *J. Clin. Periodontol.* **46**, 608–
586 622 (2019).

587 58. Loesche, W. J. Oxygen Sensitivity of Various Anaerobic Bacteria. *Appl. Microbiol.* **18**, 723–727
588 (1969).

589 59. D'souza, L. L., Lawande, S. A., Samuel, J. & Pinto, M. J. W. Effect of salivary urea, pH and ureolytic
590 microflora on dental calculus formation and its correlation with periodontal status. *J. Oral Biol.*
591 *Craniofacial Res.* **13**, 8–12 (2023).
592 60. Gaál Kovalčíková, A. *et al.* Urea and creatinine levels in saliva of patients with and without
593 periodontitis. *Eur. J. Oral Sci.* **127**, 417–424 (2019).
594 61. Nascimento, M. M., Gordan, V. V., Garvan, C. W., Browngardt, C. M. & Burne, R. A. Correlations of
595 oral bacterial arginine and urea catabolism with caries experience. *Oral Microbiol. Immunol.* **24**,
596 89–95 (2009).
597 62. Osmani, F. Can the salivary urea and stimulated saliva concentration be a marker of periodontal
598 diseases in opioid users? A case-control study. *Heliyon* **9**, (2023).
599 63. Heinrich-Weltzien, R., Kühnisch, J., Van Der Veen, M., De Josselin De Jong, E. & Stößer, L.
600 Quantitative light-induced fluorescence (QLF) - A potential method for the dental practitioner.
601 *Quintessence Int.* **34**, 181–188 (2003).
602 64. Volgenant, C. M. C. *et al.* Red fluorescence of dental plaque in children —A cross-sectional study.
603 *J. Dent.* **58**, 40–47 (2017).
604 65. Zaura, E. *et al.* On the ecosystemic network of saliva in healthy young adults. *ISME J.* **11**, 1218–
605 1231 (2017).
606 66. Kozich, J. J., Westcott, S. L., Baxter, N. T., Highlander, S. K. & Schloss, P. D. Development of a Dual-
607 Index Sequencing Strategy and Curation Pipeline for Analyzing Amplicon Sequence Data on the
608 MiSeq Illumina Sequencing Platform. *Appl. Environ. Microbiol.* **79**, 5112–5120 (2013).
609 67. Callahan, B. J. *et al.* DADA2: High-resolution sample inference from Illumina amplicon data. *Nat.*
610 *Methods* **13**, 581–583 (2016).
611 68. Evans, A. M., DeHaven, C. D., Barrett, T., Mitchell, M. & Milgram, E. Integrated, Nontargeted
612 Ultrahigh Performance Liquid Chromatography/Electrospray Ionization Tandem Mass
613 Spectrometry Platform for the Identification and Relative Quantification of the Small-Molecule
614 Complement of Biological Systems. *Anal. Chem.* **81**, 6656–6667 (2009).

615 69. Lawton, K. A. *et al.* Analysis of the adult human plasma metabolome. *Pharmacogenomics* **9**, 383–
616 397 (2008).
617 70. Kanehisa, M., Furumichi, M., Sato, Y., Ishiguro-Watanabe, M. & Tanabe, M. KEGG: integrating
618 viruses and cellular organisms. *Nucleic Acids Res.* **49**, D545–D551 (2021).
619 71. Kanehisa, M. & Goto, S. KEGG: Kyoto Encyclopedia of Genes and Genomes. *Nucleic Acids Res.* **28**,
620 27–30 (2000).
621 72. Silness, J. & Löe, H. Periodontal Disease in Pregnancy II. Correlation Between Oral Hygiene and
622 Periodontal Condition. *Acta Odontol. Scand.* **22**, 121–135 (1964).
623 73. Van der Weijden, G. A., Timmerman, M. F., Nijboer, A., Lie, M. A. & Van der Velden, U. A
624 comparative study of electric toothbrushes for the effectiveness of plaque removal in relation to
625 toothbrushing duration: Timerstudy. *J. Clin. Periodontol.* **20**, 476–481 (1993).
626 74. Aitchison, J. The Statistical Analysis of Compositional Data. *J. R. Stat. Soc. Ser. B Methodol.* **44**, 139–
627 160 (1982).
628 75. Gloor, G. B., Macklaim, J. M., Pawlowsky-Glahn, V. & Egozcue, J. J. Microbiome Datasets Are
629 Compositional: And This Is Not Optional. *Front. Microbiol.* **8**, 2224 (2017).
630 76. Bro, R. & Smilde, A. K. Centering and scaling in component analysis. *J. Chemom.* **17**, 16–33 (2003).
631 77. Chen, T. *et al.* The Human Oral Microbiome Database: a web accessible resource for investigating
632 oral microbe taxonomic and genomic information. *Database* **2010**, (2010).
633 78. Buchfink, B., Xie, C. & Huson, D. H. Fast and sensitive protein alignment using DIAMOND. *Nat.*
634 *Methods* **12**, 59–60 (2015).
635 79. Martin, M. Cutadapt removes adapter sequences from high-throughput sequencing reads.
636 *EMBnet J.* **17**, 10–12 (2011).
637 80. Kawashima, S., Katayama, T., Sato, Y. & Kanehisa, M. KEGG API: A Web Service Using SOAP/WSDL
638 to Access the KEGG System. *Genome Inform.* **14**, 673–674 (2003).
639 81. Martino, C. *et al.* Context-aware dimensionality reduction deconvolutes gut microbial community
640 dynamics. *Nat. Biotechnol.* **39**, 165–168 (2021).

82. Bro, R. The N-way Toolbox. https://nl.mathworks.com/matlabcentral/fileexchange/1088-the-n-way-toolbox.

83. Lorho, G., Westad, F. & Bro, R. Generalized correlation loadings: Extending correlation loadings to congruence and to multi-way models. *Chemom. Intell. Lab. Syst.* **84**, 119–125 (2006).

84. Borchers, H. W. & Borchers, M. H. W. Package 'pracma'. *Accessed On* **4**, (2022).

85. Schmidt, E. Über die Auflösung Linearer Gleichungen mit Unendlich Vielen Unbekannten. in *Integralgleichungen und Gleichungen mit unendlich vielen Unbekannten* (ed. Pietsch, A.) vol. 11 249–278 (Springer Vienna, 1989).

86. Kiers, H. A. L. Some procedures for displaying results from three-way methods. *J. Chemom.* **14**, 151–170 (2000).

87. Maechler, M. Finding groups in data: Cluster analysis extended Rousseeuw et al. *R Package Version* **2**, 242–248 (2019).

88. Kassambara, A. & Mundt, F. Package 'factoextra'. *Extr. Vis. Results Multivar. Data Anal.* **76**, (2017).

656 ## Tables

657 *Table 1: Overview of the correlation test results between the time-resolved subject loadings of the PARAFAC models and the*
658 *clinical parameters of gingivitis and microbiome diversity metrics. Red fluorescence was assessed at every time point. Plaque*
659 *and bleeding scores were only assessed at day -14, 0, 14 and 21 of the study. Plaque%: the percentage of sites in the mouth*
660 *that were covered in plaque. Bleeding%: the percentage of sites in the mouth that bled upon probing. RF%: the percentage of*
661 *sites that fluoresced red. Richness: the number of nonzero counts in a sample. Evenness: Shannon diversity divided by*
662 *log(richness). Benjamini-Hochberg corrected p-values of Pearson correlation tests between the subject loadings of one*
663 *component and the clinical parameters are reported (*: p≤0.05; **: p≤0.01; ***: p≤0.001).*

Sample type	Component	Plaque%	Bleeding%	RF%	Richness	Evenness
Upper jaw, lingual	1	0.024*	0.49	8.5e-6***	0.015*	0.032*
	2	0.002**	0.26	4.2e-7***	0.78	1.1e-6***
Upper jaw, interproximal	1	0.0015**	0.032*	8.1e-4***	4.4e-9***	7.0e-9***
	2	0.53	0.15	0.95	0.61	0.94
Lower jaw, lingual	1	4.9e-4***	0.14	1.2e-8***	1.6e-17***	1.5e-12***
Tongue	1	0.78	0.48	0.30	0.024*	0.057
	2	0.85	0.057	0.15	5.3e-11***	0.028*
Saliva	1	0.66	0.20	0.11	0.61	0.78
	2	0.78	0.81	0.78	7.3e-14***	8.5e-6***

664

665

666 *Table 2: Overview of all identified species per ASV cluster. ASVs within the same cluster show a similar response over time to*
667 *the gingivitis intervention. Only clustered ASVs with taxonomic annotations resolved to species level are shown.*

Sample type	Cluster	Number of members	Identified species
Upper jaw, lingual	1	9	*Actinomyces naeslundii/oris/viscosus, Kingella oralis, Rothia dentocariosa, Streptococcus cristatis/sinensis, Veillonella dispar/parvula, Veillonella atypica/dispar, Veillonella parvula/rogosae/tobetsuensis*
	2	10	*Fusobacterium canifelinus/nucleatum, Fusobacterium massiliense, Granulicetella elegans, Prevotella nanceiensis, Veillonella massiliensis*
Upper jaw, interproximal	1	3	*Rothia dentocariosa, Veillonella atypica/dispar*
	2	12	*Abiotrophia defectiva, Aggregatibacter aphrophilus/kilianii, Capnocytophaga sputigena, Lachnoanaerobaculum cf., Lautropia mirabilis, Rothia aeria/dentocariosa*
	3	5	*Corynebacterium matruchotii, Leptotrichia hofstaii, Leptotrichia shahii/wadei*
	4	11	*Aggregatibacter segnis, Capnocytophaga granulosa, Capnocytophaga leadberri, Cardiobacterium hominis, Fusobacterium canifelinus/nucelatum, Fusobacterium nucleatum, Leptotrichia buccalis, Porphyromonas pasteri*
Lower jaw, lingual	1	21	*Actinomyces georgiae/pacaensis, Aggregatibacter segnis, Campylobacter concisus, Capnocytophaga granulosa, Capnocytophaga leadbetteri, Cardiobacterium hominis, Corynebacterium matruchotii, Fusobacterium canifelinus/nucleatum, Fusobacterium nucleatum, Fusobacterium hwasooki/nucleatum/periodonticum, Lachnoanaerobaculum cf., Leptotrichia hofstadii, Porphyromonas pasteri*
	2	1	*Streptococcus salivarius* (putative)
Tongue	1	21	*Actinomyces lingnae/marseillensis/pacaensis, Capnocytophaga leadbetteri, Fusobacterium periodonticum, Granulicatella adiacens/para-adiacens, Lachnoanaerobaculum cf., Oribacterium parvum, Oribacterium sinus, Peptostreptococcus stomatis, Porphyromonas pasteri, Prevotella nanceiensis, Veillonella parvula/rogosae/tobetsuensis*
	2	20	*Actinomyces graevenitzii, Alloprevotella rava, Atopobium parvulum, Lachnoanaerobaculum orale/saburreum, Prevotella histicola, Prevotella jejuni/melaninogenica, Prevotella salivae, Prevotella veroralis, Rothia mucilaginosa, Stomatobaculum longum*
Saliva	1	9	*Granulicetella adiacens/para-adiacens, Porphyromonas pasteri, Rothia aeria/dentocariosa*
	2	21	*Actinomyces graevenitzii, Atopobium parvulum, Campylobacter concisus, Lachnoanaerobaculum orale/saburreum, Prevotella histocola, Prevotella jejuni/melanogenica, Prevotella salivae, Rothia mucilaginosa, Stomatobaculum longum, Veillonella atypica/dispar*

668